



# City Research Online

## City St George's, University of London

**Citation:** Rahman, B. M., Markides, C., Uthman, M., Quadir, A., Kejalakshmy, N. & Themistos, C. (2014). Characterization of low-loss waveguides and devices for terahertz radiation. *Optical Engineering (OE)*, 53(3), 031210. doi: 10.1117/1.oe.53.3.031210

This is the published version of the paper.

This version of the publication may differ from the final published version. To cite this item please consult the publisher's version.

**Permanent repository link:** <https://openaccess.city.ac.uk/id/eprint/12215/>

**Link to published version:** <https://doi.org/10.1117/1.oe.53.3.031210>

**Copyright and Reuse:** Copyright and Moral Rights remain with the author(s) and/or copyright holders. Copies of full items can be used for personal research or study, educational, or not-for-profit purposes without prior permission or charge, unless otherwise indicated, provided that the authors, title and full bibliographic details are credited, a hyperlink and/or URL is given for the original metadata page and the content is not changed in any way. For full details of reuse please refer to [City Research Online policy](#).

# Optical Engineering

[SPIDigitalLibrary.org/oe](http://SPIDigitalLibrary.org/oe)

## **Characterization of low-loss waveguides and devices for terahertz radiation**

B. M. Azizur Rahman  
Christos Markides  
Muhammad Uthman  
Anita Quadir  
Namassivayane Kejalakshmy  
Christos Themistos

# Characterization of low-loss waveguides and devices for terahertz radiation

B. M. Azizur Rahman,<sup>a</sup> Christos Markides,<sup>b</sup> Muhammad Uthman,<sup>a</sup> Anita Quadir,<sup>a</sup> Namassivayane Kejalakshmy,<sup>a</sup> and Christos Themistos<sup>b</sup>

<sup>a</sup>City University London Northampton Square, School of Engineering and Mathematical Sciences, London EC1V 0HB, United Kingdom

<sup>b</sup>Frederick University, School of Engineering and Applied Sciences, Y. Frederickou 7, 1036, Nicosia, Cyprus

**Abstract.** A rigorous full-vectorial modal solution approach based on the finite element method is used to find the propagation properties of terahertz (THz) waveguides, such as photonic crystal fibers, quantum cascaded lasers, plasmonic waveguides, power splitters, and narrow-band filters. Design approaches to reduce the modal loss due to the material and leakage loss in photonic crystal fibers and in metal-coated hollow-glass plasmonic waveguides have also been considered. The plasmonic confinement and gain threshold of quantum cascaded lasers used as THz sources and the chromatic dispersion in plasmonic waveguides are also presented. © 2014 Society of Photo-Optical Instrumentation Engineers (SPIE) [DOI: 10.1117/1.OE.53.3.031210]

Keywords: terahertz waveguides; terahertz devices; finite element method; finite difference time domain.

Paper 131049SS received Jul. 11, 2013; revised manuscript received Jan. 17, 2014; accepted for publication Feb. 3, 2014; published online Mar. 10, 2014.

## 1 Introduction

The terahertz (THz) region occupies a large portion of the electromagnetic spectrum, located between the microwave and optical frequencies, and is normally defined as the band ranging from 0.1 to 10 THz. In recent years, this intermediate THz radiation band has attracted considerable interest because it offers significant scientific and technological potential for applications in many fields, such as sensing,<sup>1</sup> imaging,<sup>2</sup> and spectroscopy.<sup>3</sup> However, waveguiding in this intermediate spectral region is a major challenge, and strong dielectric and conductive losses in the THz frequency range have been a major problem for waveguiding. The conventional guiding structures exemplified by microstrips, coplanar striplines, and coplanar waveguides<sup>4</sup> are highly lossy and dispersive. However, so far the most promising dielectric waveguides have been the use of photonic crystal fibers at THz frequencies<sup>5,6</sup> and metal-coated guides<sup>7</sup> at THz frequencies. In this paper, various types of practical dielectric and metal-coated waveguides are evaluated, including their modal loss and dispersion, and design optimization of quantum cascade lasers, multimode interference coupler (MMI)-based power splitters, and narrow-band filters are also presented by using a full-vectorial H-field finite element method.<sup>8</sup> We have used an in-house code based on this H-field formulation,<sup>8</sup> which has been cited more than 600 times, and following 30 years of continuous development and refinement, this may be one of the best codes for modal solutions of a wide range of optical waveguides. Our results have been used for benchmarking by others.<sup>9</sup>

## 2 Photonic Crystal Fibers: THz Waveguides

Dielectric waveguides in silica, silicon, polymer, and other semiconductor materials have been widely used at optical frequencies; however, most of these materials are very lossy at the lower THz frequency range. So far most of the

photonic crystal fibers (PCFs) that have been considered have been fabricated from silica or non-silica glasses due to their low loss in the optical frequency range, but the material loss of silica is prohibitively high at THz frequencies. However, only recently, Han et al.<sup>5</sup> have fabricated a PCF for THz using high-density polyethylene with modal loss values of 0.2 cm<sup>-1</sup>, and Goto et al.<sup>6</sup> have reported a PCF-like waveguide using Teflon tubes and filaments with loss values of 0.5 cm<sup>-1</sup>, showing their potential.

A typical PCF cross-section with a triangular array of holes is shown in Fig. 1. The structure predominantly consists of periodic air-holes with diameter  $d$ , and the pitch length between the two nearest holes is  $\Lambda$ . In this work, a refractive index value  $n_g = 1.444$  is considered, at the operating frequency of 1.2 THz (wavelength 0.25 mm).

Variations of the effective indices for both the fundamental  $H_{11}^x$  and the second  $H_{21}^x$  modes for  $d/\Lambda = 0.9$  are shown in Fig. 2. It can be noted that for both the modes, the effective indices reduce monotonically as the pitch length is reduced. The variation of the  $n_{\text{fsm}}$  value with the pitch length is also shown by a chained line for  $d/\Lambda = 0.9$  at 1.0 THz. The  $n_{\text{fsm}}$  represents a frequency-dependent equivalent index of the perforated cladding region, and this was calculated by solving a unit cell problem with periodic boundary conditions implemented around all four sides. It can be observed that the effective index curve for the  $H_{21}^x$  mode crosses the  $n_{\text{fsm}}$  line at a pitch length of  $\Lambda_c = 0.24$  mm, so when the pitch length is reduced below 0.24 mm, the second mode cannot continue to be guided. On the other hand, the effective index for the fundamental  $H_{11}^x$  mode also crosses the  $n_{\text{fsm}}$  line, but at  $\Lambda_c = 0.11$  mm. So, a PCF with  $d/\Lambda = 0.9$  and pitch length between 0.11 and 0.24 mm would be strictly single moded. By controlling the  $d/\Lambda$  ratio and the pitch length, the modal properties of such low-loss PCFs at THz operating frequency can easily be controlled.

The modal loss of a guided mode in a PCF is due to the combination of the material loss and the leakage loss.

\*Address all correspondence to: Christos Themistos, E-mail: [c.themistos@cytanet.com.cy](mailto:c.themistos@cytanet.com.cy)

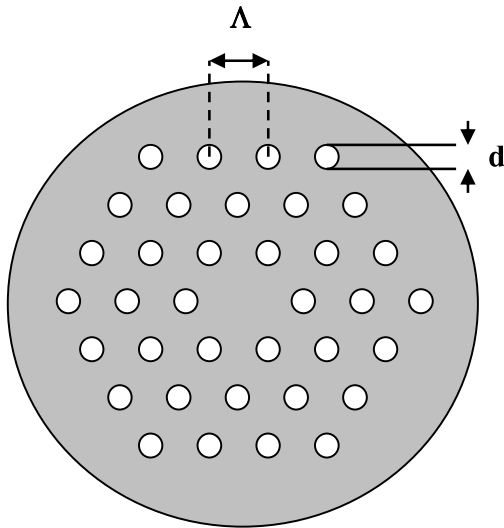


Fig. 1 Cross-section of a photonic crystal fiber.

The material loss arises due to the complex refractive indices of the waveguide materials, and the leakage loss arises due to the modal index being lower than the surrounding high-index cladding regions. In this work, perfectly matched layers (PMLs)<sup>10</sup> are incorporated around the orthodox computational window. For this study, a PCF with parameter  $d/\Lambda = 0.5$  is used. To consider the effect of the loss tangent, three different values of the  $n_i$  (the imaginary part) have been considered.

Figure 3 shows the loss mechanism in a PCF. In the absence of any material loss, for  $n_i = 0$ , the leakage loss is shown by a solid line. It can be observed that as the pitch length is reduced, the leakage loss increases almost linearly from a very low loss value. In the case of  $n_i = 0.00119$ , the total loss included both the leakage loss and the material loss, which is shown by a dashed line. At a higher pitch value, when the leakage loss is negligible, the total loss is mainly attributable to the material loss. Although it can be observed that by reducing the pitch value below 0.2 mm confinement in more lossy solid dielectric can be reduced, however, this figure also shows that the leakage loss (and bending loss, which is not shown here) of such waveguides will also be very high.

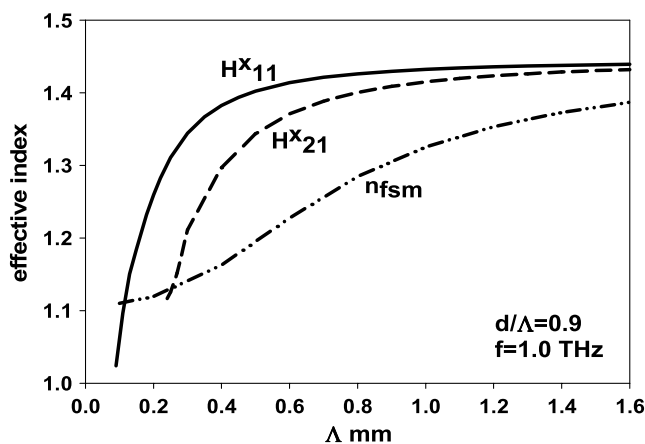


Fig. 2 Variation of the effective indices with the pitch length  $\Lambda$ .

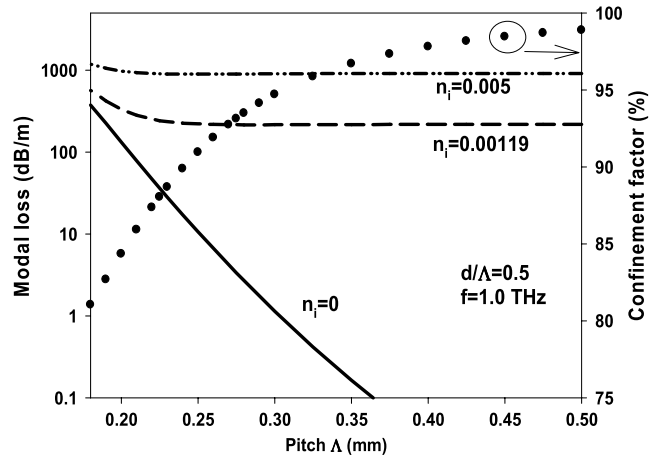


Fig. 3 Material and leakage losses of PCF.

Since at present the available dielectric materials at THz frequencies are considerably lossy, a novel design approach is considered next, where a porous core PCF is considered. As the waveguide dimensions for THz frequency are considerably bigger than those for the optical wavelength, it would be relatively easy to fabricate such a microstructured core. Two different  $d/\Lambda$  values are used for core ( $d/\Lambda_i$ ) and cladding ( $d/\Lambda_o$ ), and for cladding, this value has to be smaller to have higher equivalent index in the core for wave guidance.

Variation of the power fraction in the air-region of the porous core is shown in Fig. 4. As shown in this figure, the power confinement can be increased to 35% in the low-loss air-holes of the cores, and additionally another 25% in the cladding air-holes,<sup>11</sup> but this is not shown here. With this arrangement, >60% power can be in the low-loss air region, which will reduce the modal loss by 60% for a more flexible dielectric waveguide structure.

Among the various THz waveguides that have been suggested, the metal-clad waveguides supporting surface plasmon modes show the greatest promise as low-loss waveguides for use both in active components and as passive waveguides. Several waveguide structures incorporating metallic layers have been reported, such as low-loss and flexible hollow polycarbonate waveguide with copper and

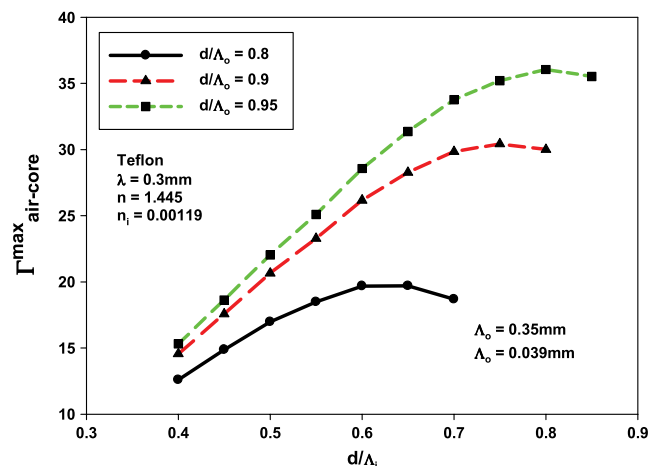


Fig. 4 Variation of power confinement in porous air-holes in the core region with the pitch length  $\Lambda$ .

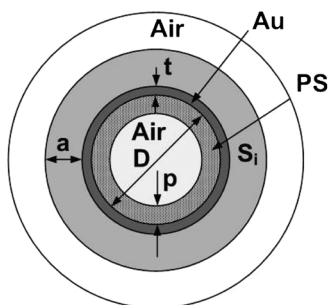


Fig. 5 Metal-coated hollow glass waveguide.

dielectric inner coatings, deposited by using a liquid chemistry approach.<sup>12</sup>

A metal-coated hollow glass waveguide (HGW)<sup>13</sup> with an inner silver/polystyrene (PS) coating, as shown in Fig. 5, is considered for the better understanding of the various loss mechanisms and subsequent design optimization of a low-loss THz waveguide. For this waveguide, the thickness of the silica tube ( $s$ ) is taken as 0.5 mm and the bore diameter ( $D$ ) of the HGW as 2 mm. The thickness of the silver cladding ( $t$ ) and PS layer ( $p$ ) are taken as  $t \mu\text{m}$  and  $p \mu\text{m}$ , respectively. The complex refractive index of the PS, the silver metal cladding layers, and the silica ring are taken as  $n_p = 1.58 - j0.0036$ ,  $n_m = 308 - j532$ , and  $n_s = 1.96 - j0.0061$ , respectively, at an operating frequency of 2.5 THz. At this frequency, as the air is also not absolutely loss-free; to represent this loss factor, its complex refractive index is taken as  $1.0 - j1.1 \times 10^{-6}$ .

There are two metal/dielectric interfaces, which can support surface plasmon modes (SPMs), one the outer silver/silica boundary and the other at the inner silver/PS (or air, when  $p = 0 \mu\text{m}$ ) boundary. This waveguide supports two SPMs along these two metal/dielectric interfaces. The refractive indices of the inner and outer cladding materials being very different, the two SPMs have widely different propagation constants and they do not interact with each other. However, at the right- and lefthand sides of the metal/dielectric interfaces, when the same electric-wall boundary condition is imposed, the  $H_x$  field is forced to be zero at the metal boundary and no SPM exists. Another mode with the dominant  $H_y$  field would form a similar SPM, however, at the left and the right interfaces. The  $H_y$  field profile of this mode is similar to the  $H_x$  field profile, but rotated by 90 deg. These two modes have identical propagation constants and being degenerate, they can be superimposed to form radially polarized (RP)-like modes. The superposition of their field profiles indicates a rotationally symmetric profile similar to those reported for dielectric clad metal waveguides supporting SPMs at optical frequencies.<sup>14</sup>

The loss values of the fundamental plasmonic mode increases with the PS thickness and is not shown here. The attenuation characteristics of the  $\text{RP}^{02}$  mode, with the variation of the PS thickness, for a silver thickness  $t = 0.4 \mu\text{m}$  is shown in Fig. 6, where the loss contribution of the PS and silver layers has also been examined. As can be seen from the above characteristics, the total attenuation shows a maximum and a minimum loss at a PS thickness of  $\sim 1$  and  $13 \mu\text{m}$ , respectively. The attenuation curves due to the PS and the silver layer exhibit similar trend with the total attenuation. Throughout the range of PS

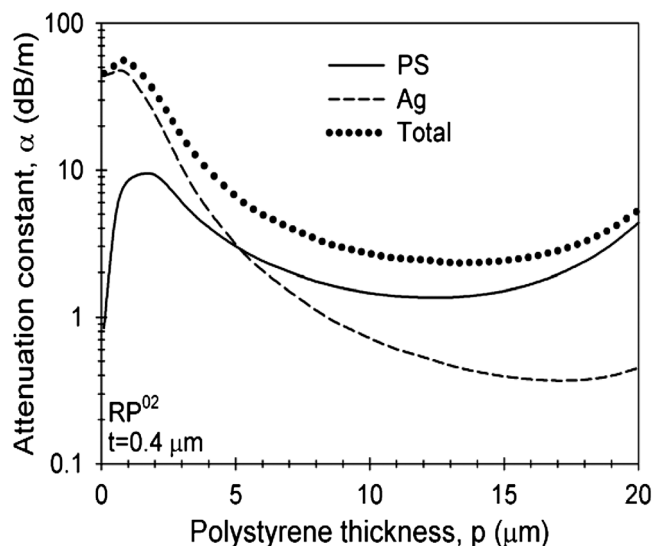


Fig. 6 Attenuation constant with the polystyrene thickness  $p$  for  $t = 0.4 \mu\text{m}$ .

thicknesses examined, the optical power confinement in the inner air-core is of the order of 99.9%, thus contributing a constant attenuation of  $\sim 0.25 \text{ dB/m}$ . For a PS thickness  $< 5 \mu\text{m}$ , the total attenuation is affected mainly due to the metal attenuation, but as the PS thickness increases above  $5 \mu\text{m}$ , the total attenuation is mainly governed by the loss in the PS layer. This mode shows a greater promise to achieve low-loss guidance through a metal clad dielectric waveguide. It would also be easier to couple this mode since the field profile is also very close to a Gaussian shape.<sup>13</sup> The modal loss of this waveguide, when design is optimized, is significantly lower than most of the THz waveguides reported so far, as most of the power is being guided in the central air-hole region.

Next this novel approach is considered to design and optimize a low-loss rectangular core metal waveguide, as shown in Fig. 7. If we consider that its height and widths are different, then the polarized modes will not be degenerate. In our more recent work,<sup>15</sup> we have shown that, similarly, a polarization maintaining rectangular air-core dielectric-clad metal-coated waveguide can also be less lossy. A thin metal coating would support plasmonic modes, but these are relatively lossy. However, a Teflon coating on

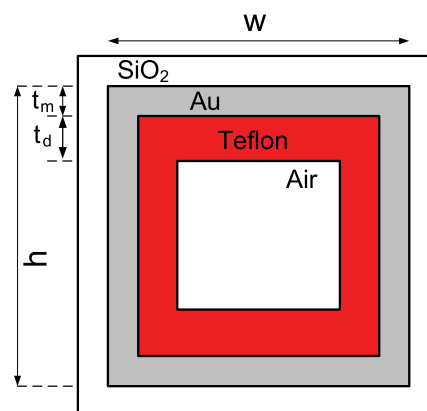


Fig. 7 Low-loss rectangular core metal waveguide.

the gold layer can draw field away from the lossy conducting layer and loss may reduce considerably. Figure 8 shows the variation of the loss value with the Teflon thickness for the  $H_{12}^x$  mode in an air-core  $1 \times 0.6$  mm rectangular waveguide with  $0.7 \mu\text{m}$  gold coating at 2.5 THz. It can be seen that at the optimum 21- $\mu\text{m}$  Teflon thickness, the loss value can be 3.5 dB/m, one of the lowest reported so far.<sup>16</sup> The loss value can be further reduced by increasing the core dimension (W and h), but this would allow higher-order modes to be guided. The evolution of third-order mode for no Teflon coating ( $t_d = 0$ ) to a near-Gaussian profile for  $t_d = 18\text{-}\mu\text{m}$  Teflon coating are shown as insets. The near-Gaussian profile would be useful for efficient coupling of this mode from an external source. The two-dimensional (2-D)  $H_x(x, y)$  profile for Teflon coated (with  $t_d = 18 \mu\text{m}$ ) is also shown as another inset.

Moreover, the finite difference time domain (FDTD) method is used to obtain the dispersion characteristics of the waveguide. A 2-D formulation of the FDTD method with PML absorbing boundary conditions is used to study the electric field distribution along the axis of propagation of the waveguide. A Gaussian pulse was launched into the waveguide as shown in Fig. 9(a), and the electric field at various points along the direction of propagation was monitored. The electric field distribution for an input profile with spot size 80% of the width of the rectangular waveguide, sampled

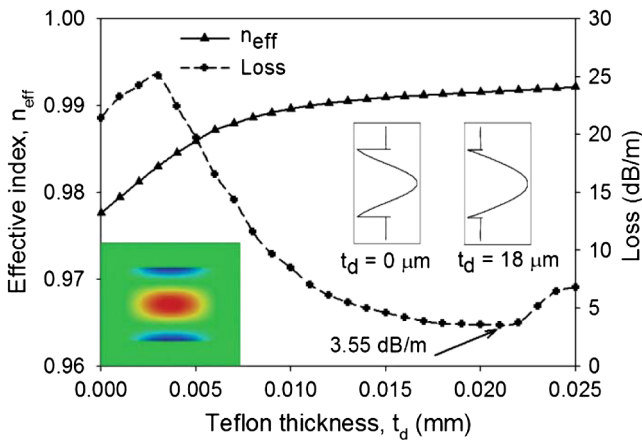


Fig. 8 Effective index and loss with Teflon thickness for the  $H_{10}^x$  mode.

at 2.5 THz using discrete Fourier transform, has been calculated and is also presented in Fig. 9(b). The waveguide supports a propagating fundamental mode with high electric field value along the center of the waveguide. The propagating fundamental mode can be supported with small losses as the spot size of the input pulse is decreased to 90 and 80%, respectively. After that threshold, as the spot size decreases there is a rapid decay in the electric field with significant losses and the plasmonic behavior of the waveguide rapidly deteriorates.

The dispersion parameters of the plasmonic waveguide can be calculated from the time-domain values of the normalized electric fields, and the full-width half-maximum (FWHM) pulse width in picosecond for each of the monitors can be determined. The FWHM pulse spread is calculated at various points along the direction of propagation of the waveguide. The FWHM pulse spread with propagation distance for different input pulse spot sizes (85 to 95%) is plotted in Fig. 10. As the propagation distance increases, the FWHM pulse spread increases exponentially as an indication of the dispersion that the electric field undergoes as it travels through the waveguide.

Quantum cascading lasers<sup>16</sup> are emerging as efficient high-power THz sources for many important applications, such as imaging and sensing. However, for the THz

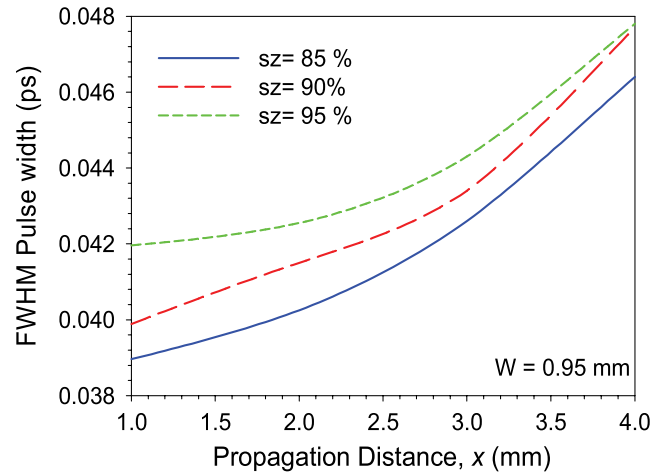


Fig. 10 Full width half maximum pulse spread with propagation distance for different input pulse spot size.

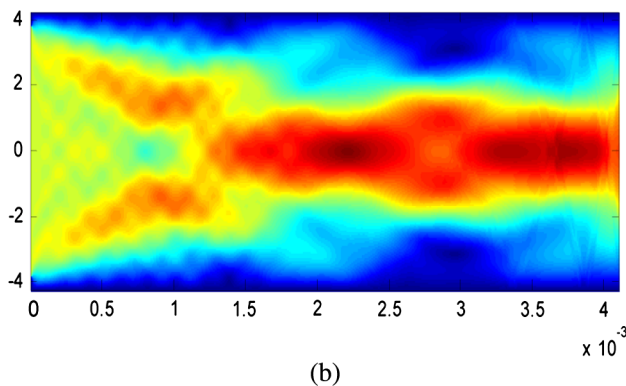
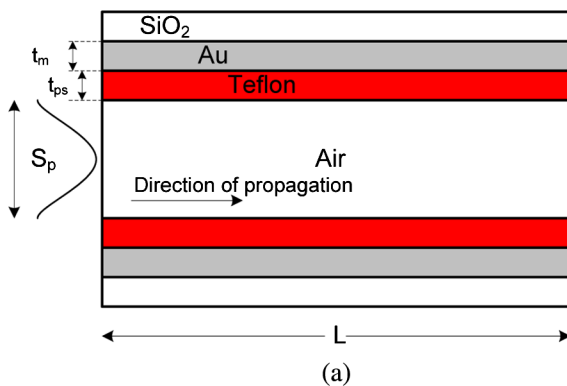
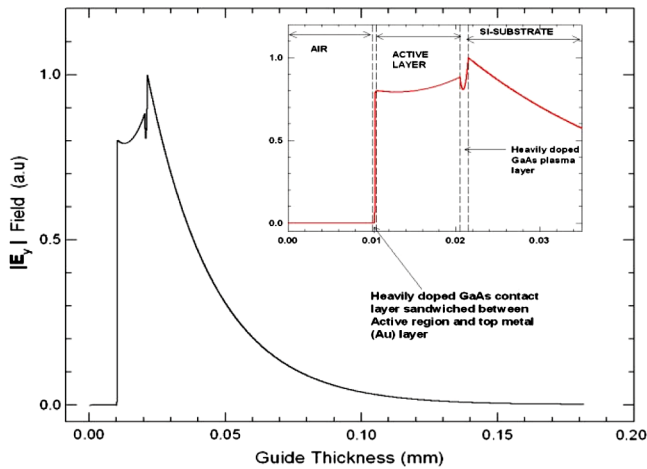


Fig. 9 (a) Gaussian pulse launched into the plasmonic waveguide. (b) Field distribution for 80% spot size Gaussian pulse.



**Fig. 11** Field profile of  $E_y$  mode in a terahertz quantum cascade laser. The field inside the confinement layers is shown in the inset.

frequency, the wavelength is large, and it is not possible to grow the semiconductor materials comparable to the operating wavelength. For this reason, for THz quantum cascaded laser (QCL) often smaller heights need to be considered and plasmonic confinement is used in that direction. The plasmonic confinement in the vertical direction is shown in Fig. 11, which clearly shows the mode formation at the metal–dielectric interfaces. However, it is easily possible to have a wider guide, so mostly dielectric confinement is used in horizontal direction.

The gain threshold for such QCL is shown in Fig. 12. Because of the wider guides, the gain threshold difference between the fundamental and higher-order (lateral) modes are very small. This allows possibility of mode hopping for any external changes. A novel design approach is considered<sup>17</sup> using slotted upper metal clad to enhance the gain threshold of the higher-order modes. Figure 13 clearly shows that gain threshold of the higher-order modes are increased for slotted-electrode designs. For the future THz system, it is essential to design various integrated guided-wave components. In that spirit, it is shown here that a

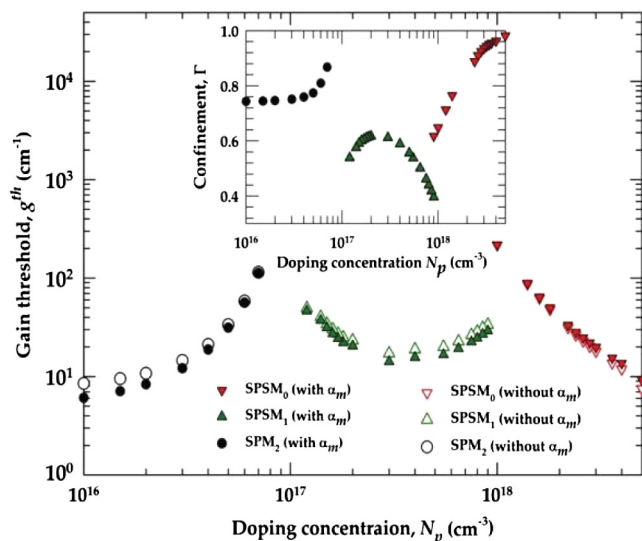


**Fig. 12** Gain threshold of several plasmonic modes.

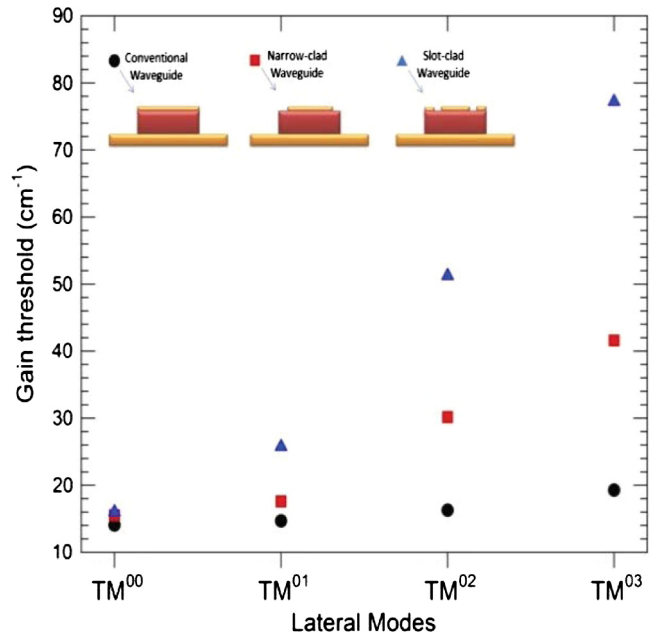


**Fig. 13** Gain threshold of the lower-order modes for different waveguides.

compact power splitter can be designed by using the MMI principle.

In Fig. 14, it is shown here that an efficient power splitter can be designed by using a 35- $\mu\text{m}$ -long multimoded section.<sup>18</sup>

Finally, a THz frequency range band-stop filter for molecular sensing,<sup>19</sup> where two 5- $\mu\text{m}$ -wide band-stop filter stubs with lengths of 192 and 83  $\mu\text{m}$  are placed 400  $\mu\text{m}$  apart along the direction of propagation, as shown in the right inset of Fig. 15, has been considered. Initially the above device has been simulated without a PS film on top of the metal layer, using the FDTD approach, and the variation of the insertion loss with the frequency is presented in Fig. 15. As can be seen from the frequency response, the device exhibits two resonant frequencies due to the stubs at  $\sim 600$  and 800 GHz, with a minimum insertion loss of  $\sim -55$  and  $-30$  dB.

The effect of the presence of PS along the metal surface of the microstrip line on the propagation, attenuation characteristics, and frequency response in band-stop filter design has also been investigated. The insertion loss of the microstrip loaded with PS coating clearly shows a change in the value of the insertion loss. As the PS coating is increased, the insertion loss increases for the 30- $\mu\text{m}$ -wide microstrip line, but is not presented here. In order to observe the shifts in frequency as the PS coating is increased, a closer look is

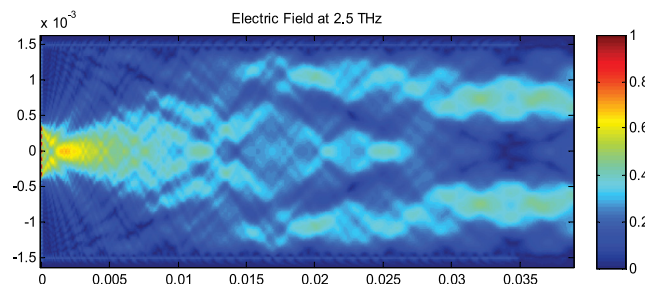


**Fig. 14** FDTD simulation of the 3 mm MMI 3 dB coupler.

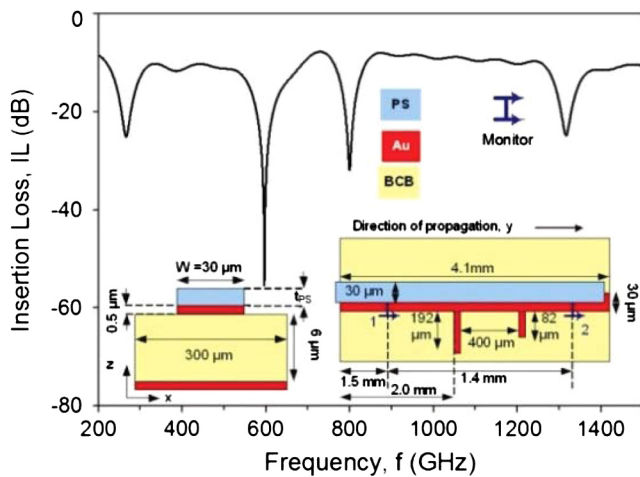


Fig. 15 Insertion loss with frequency for the microstrip filter.

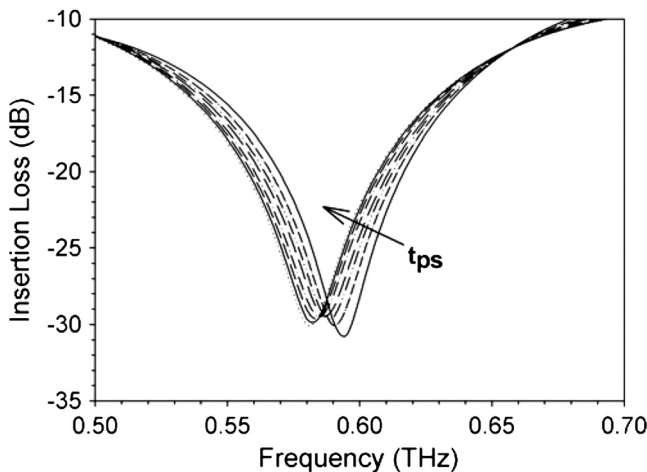


Fig. 16 Insertion loss of the microstrip structure for different values of polystyrene thickness (0 to 15  $\mu\text{m}$ ).

required, and therefore, the insertion loss is plotted against the PS coating thickness for the 600-GHz filter, as shown in Fig. 16.

For a PS thickness of 2  $\mu\text{m}$ , the insertion loss is initially reduced; however, as the PS thickness increases further, the insertion loss of the above material reaches the value obtained for the structure without the PS film. Furthermore, as the PS thickness increases, the frequency of the peak insertion loss reduces, as presented in Fig. 16.

### 3 Conclusion

A finite-element approach, based on a full-vectorial  $\mathbf{H}$ -field formulation, has been used to study the detailed modal properties of dielectric and metal clad waveguides operating in the THz frequency range. It is also shown here that by using porous core, the effect of material loss can be reduced significantly. It is also shown by using a thin but optimized

dielectric overlayer plasmonic loss in a hollow-core waveguide can also be reduced. It is also shown here that by using a novel slot-type electrode, the differential loss of the higher-order modes can be significantly increased to reduce mode hopping. Finally, simple guided-wave devices, such as power splitters and band-pass filters, are also presented here by using the FDTD approach. The design approach used here can be extended to optimize not only THz waveguides but also more advanced guided-wave devices for possible THz integrated circuits of the future. The finite element method approach is particularly more suitable to represent plasmonic structures when metal layers may be several orders thinner than dielectric regions.

### References

1. R. H. Jacobsen, D. M. Mittleman, and M. C. Nuss, "Chemical recognition of gases and gas mixtures with terahertz waves," *Opt. Lett.* **21**(24), 2011–2013 (1996).
2. Q. Chen et al., "Near-field terahertz imaging with a dynamic aperture," *Opt. Lett.* **25**(15), 1122–1124 (2000).
3. J. Q. Zhang and D. Grischkowsky, "Waveguide terahertz time-domain spectroscopy of nanometer water layers," *Opt. Lett.* **29**(14), 1617–1619 (2004).
4. M. Y. Frankel et al., "Terahertz attenuation and dispersion characteristics of coplanar transmission-lines," *IEEE Trans. Microw. Theory Tech.* **39**(6), 910–916 (1991).
5. H. Han et al., "Terahertz pulse propagation in plastic photonic crystal fiber," *Appl. Phys. Lett.* **80**(15), 2634–2636 (2002).
6. M. Goto et al., "Teflon photonic crystal fiber as terahertz waveguide," *Jpn. J. Appl. Phys.* **43**(Part 2), L317–L319 (2004).
7. R. W. McGowan, G. Gallot, and D. Grischkowsky, "Propagation of ultrawideband short pulses of terahertz radiation through submillimeter diameter circular waveguides," *Opt. Lett.* **24**(20), 1431–1435 (1999).
8. B. M. A. Rahman and J. B. Davies, "Finite-element analysis of optical and microwave waveguide problems," *IEEE Trans. Microw. Theory Tech.* **32**(1), 20–28 (1984).
9. G. R. Hadley and R. E. Smith, "Full-vector waveguide modeling using an iterative finite-difference method with transparent boundary conditions," *J. Lightwave Technol.* **13**(3), 465–469 (1995).
10. N. Kejalakshmy et al., "Characterization of single-polarization single-mode photonic crystal fiber using full-vectorial finite element method," *Appl. Phys. B* **93**(1), 223–230 (2008).
11. M. Uthman et al., "Design and characterization of low-loss porous-core photonic crystal fiber," *IEEE Photonics J.* **4**(6), 2314–2325 (2012).
12. J. A. Harrington et al., "Hollow polycarbonate waveguides with inner Cu coatings for delivery of terahertz radiation," *Opt. Express* **12**(21), 5263–5268 (2004).
13. C. Themistos et al., "Characterization of silver/polystyrene (PS)-coated hollow glass waveguides at terahertz frequency," *J. Lightwave Technol.* **25**(9), 2456–2462 (2007).
14. C. Themistos, B. M. A. Rahman, and K. T. V. Grattan, "TM/TE modal solution for sub-micron lossy metal-clad optical fibers," *IEE Proc. Optoelectron.* **145**(3), 171–177 (1998).
15. B. M. A. Rahman et al., "Characterization of plasmonic modes in a low-loss dielectric-coated hollow core rectangular waveguide at terahertz frequency," *IEEE Photonics J.* **3**(6), 1054–1066 (2011).
16. J. Faist et al., "Quantum cascade laser," *Science* **264**(5158), 553–556 (1994).
17. H. Tanvir, B. M. A. Rahman, and K. T. V. Grattan, "Impact of 'ghost' mode interaction in terahertz quantum cascade lasers," *IEEE Photonics J.* **3**(5), 926–935 (2011).
18. C. Markides et al., "Multimode interference 3 dB splitters in hollow core metallic waveguides for low loss THz wave transmission," *IEEE J. Sel. Topics Quantum Electron.* **19**(1), 8500606–8500704 (2013).
19. J. Cunningham et al., "Terahertz frequency range band-stop filters," *Appl. Phys. Lett.* **86**(21), 213503 (2005).

Biographies of the authors are not available.